nzsee
NEW ZEALAND SOCIETY FOR EARTHQUAKE ENGINEERING

Design considerations for buckling restrained braces in timber frames subject to out of plane deformations

W. P. Dorrance, M. A. Huang, G. A. MacRae, M. Bashiri
University of Canterbury, Christchurch, New Zealand.

M-H Li
University of British Colombia, Vancouver, Canada.

ABSTRACT

Buckling restrained braces (BRBs) can improve the in-plane seismic performance of timber frames but little is understood about the frame out-of-plane (OOP) performance. This research evaluates the performance of chevron BRBs subjected to OOP drifts in a single storey timber frame. Timber connection rotational stiffnesses were first obtained using finite element, and beam-on-elastic-foundation, methods. Then, a 3D elastic analysis was used to analyse the BRB system global response considering the timber beam OOP and torsional stiffnesses, and the timber connection rotational stiffnesses. A new, and rational, approach is then applied to assess the likelihood of component yield within the BRB system outside the core yield zone.

It was found that for the BRB frame considered with unstiffened gusset plates, an OOP drift of only 0.83% could be achieved before yield occurred in the gusset plates. With highly stiffened gusset and connection plates, the maximum OOP drift was 1.5%. However, for a moderately stiffened gusset and connection plates, the OOP drift capacity was 1.66% highlighting the importance of finding the "sweet spot" in BRB system stiffness.

1 INTRODUCTION

Mass timber frames have become more popular around the world as a result of governmental directives. However, the height of mass timber structures are restricted in high seismic regions due to their limited ductility capacity. The introduction of buckling restrained braces (BRBs) within timber structures may result in a more ductile structural system, when compared to traditional timber braces, as indicated by tests at the University of Canterbury by Dong (2021). This may permit taller timber buildings.

Currently, buckling restrained braces are generally permitted to be deployed in buildings after they have shown satisfactory in-plane test performance. However, out-of-plane (OOP) deformations may negatively affect BRB frame performance, especially in the first storey of buildings where BRBs are connected to stiff foundations. This is because stiff OOP base connections can lead to BRB OOP moment demands which

cause (i) increased BRB compression forces, and (ii) undesirable yielding in the BRB system outside the specified core yield zone which can reduce the deformation capacities. Accepted methods for considering OOP actions on BRB frames are still under development, but a simple and rational methodology developed by MacRae et al. (2022) has been proposed to prevent BRB system yield outside the yield zone considering OOP actions on BRBs in D-braced steel frames. There has been no similar study on OOP effects of BRBs in timber frames, or in chevron configuration frames.

Based on the above, it may be seen that if engineers wish to design tall timber frames, which may have BRBs in a chevron configuration, there is a need for design guidance.

The research aims to address this need by seeking answers to the following questions:

- Can the behaviour of out-of-plane bending of BRBs be understood and modelled?
- Can the relevant properties of the timber frame connections be modelled?
- How does BRB gusset plate and timber frame stiffness affect OOP BRB frame behaviour?
- What are the lessons from the finding from answers to the questions above for designers?

2 LITERATURE REVIEW

2.1 Acceptance Criteria

For optimal BRB performance considering out-of-plane deformations, MacRae et al. (2022) propose that two criteria are met: (i) an axial check and (ii) a combined axial/flexural check.

The maximum possible BRB axial force , C_{max}, is determined by Equation (1) according to AISC341 F4-2a (2016). Here, ω is the ratio of the peak measured tension strength at twice the predicted brace design level displacement to the actual measured yield strength, β is the ratio of the peak compression strength to the peak tension strength, ϕ_{om} is the overstrength factor for steel = 1.1, and P_{ysc} is the tensile strength of the yield zone.

$$C_{max} = \omega\beta\phi_{om}P_{ysc} \quad (1)$$

The axial buckling check, given in Equation (2), should consider the maximum BRB system flexibility (i.e. the lowest stiffness parameters at the end of the BRB system which the BRB is at its maximum elongation) as this will result in lower, and more conservative, estimates of BRB elastic buckling load, P_e, as determined from elastic critical load analysis.

$$C_{max} < 0.285P_e \quad (2)$$

For the combined axial/flexural check, the maximum BRB system stiffness results in the largest moment demands. Furthermore, Cui (2021) shows that out-of-plane deformations can increase the BRB compressive strength by a factor of 1.3. A modified maximum possible compressive strength, $C_{max,0}$, allowing for this is shown in Equation (3). To prevent yield occurring in any component along the length of the BRB member, apart from in the specified core yield zone, the linear axial force-moment interaction given by Equation (4) has been proposed, where M_i^* is the moment demand for each component, i. $M_{y,i}$ and $P_{n,i}$ are the moment and axial resistance, respectively for separate components along the length of the BRB system, and ϕ = 0.9 from NZS3404 (1997). The axial strength, $P_{n,i}$, and moment capacity, $M_{y,i}$, shown in (4) can be determined using Section 2.2.

$$C_{max,0} = 1.3C_{max} \quad (3)$$

$$\frac{C_{max,0}}{\phi P_{n,i}} + \frac{M_i^*}{\phi M_{y,i}} < 1 \quad (4)$$

2.2 BRB Component Strength

MacRae et al. (2022) propose the NZS3404 column curve approach be used to determine the inelastic axial strength, $\phi P_{n.i}$ for each component, i, in the BRB system. The strength, with $k_f = 1$ can be found using the slenderness parameter λ_n according to NZS3404 (1997) Clause 6.3.4b as shown in Equation (5) where $P_{yi} = F_y A_i$, F_y is the steel yield stress, and A_i is the cross-section area for each component. A full derivation Equation (5) is given in MacRae et al. (2022).

$$\lambda_{n,i} = \frac{kl}{r}\sqrt{\frac{F_y}{250MPa}} = 90\sqrt{\frac{P_{y,i}}{P_e}} \tag{5}$$

Moment capacity, $\phi M_{n.i}$ is determined using Equation (6) where Z is the component section elastic modulus.

$$\phi M_{n,i} = \phi Z_i F_y \tag{6}$$

2.3 Gusset Plate Parameters

Gusset plate properties, such as OOP second moment of area, I_g, and elastic section modulus, Z_g, and area, A_g, are required to determine the system elastic buckling load and yield strength. Here, a simple and rational method is used which splits the gusset plate into 3 strips, each with a tributary area equal to the plate thickness t_g multiplied by one half of the connection width b_c (MacRae, 2022). Using this approach, A_g and Z_g are given in Equations (7) and (8) respectively.

$$A_g = 1.5 t_g b_c \tag{7}$$

$$Z_g = \frac{1.5 b_c t_g^2}{6} \tag{8}$$

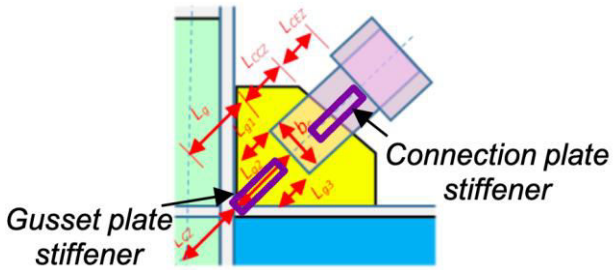

Also I_g is determined using the 3 strip element lengths, L_{g1}, L_{g2}, L_{g3} as shown in Figure 1 according to Equation (9) where $I_{g1,2,3}$ is the moment of inertias for each strip element.

$$I_g = L_g^2\left(\frac{I_{g1}}{L_{g1}^2} + \frac{I_{g2}}{L_{g2}^2} + \frac{I_{g3}}{L_{g3}^2}\right)$$

Figure 1: Gusset plate strips (MacRae et al. 2022)

2.3.1 Effect of Rectangular Stiffeners

Gusset and connection stiffening plates increase the axial capacity, ϕP_n, and moment capacity, ϕM_n. However, stiffeners also increase the element stiffness EI which increases the moment demand, M^*. Doubling the rectangular stiffener depth, d increases EI by 8 times (since $I = bd^3/12$) but increases ϕM_n by only 4 times ($M_n = bd^2/6 \times F_y$) (MacRae et al. 2022). This implies that increasing the stiffener depth may increase OOP moment demands more than increase the OOP plate moment capacity. If gusset plates and connections are very flexible, then they may be susceptible to buckling under axial force, and if they are very stiff, then the plates may yield under OOP deformations. This shows the importance of finding the 'sweet spot' for the gusset and connection plate stiffness to obtain the best OOP performance.

2.4 Restraint Parameters

BRB end restraints influence the BRB system response to out-of-plane deformations. Stiffer restraints increase the moment demands, M^*, while more flexible restraint conditions decreases the elastic buckling load, P_e. Rotational restraint at the chevron brace-beam connection is dependent on the lateral and torsional stiffnesses of the beam, and the twisting stiffness of the beam-column connection (which also considers the effect of the slab-to-beam connection). Methods to determine some of the stiffness properties affecting the BRB system performance are shown below.

2.4.1 Timber Beam Torsional Stiffness

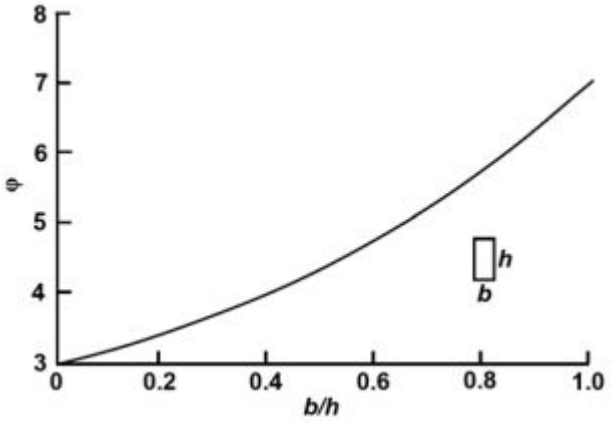

The Wood Handbook (FPL, 2010) states that the torsional rigidity, C, of a rectangular timber member is obtained using Equation (10) where the average shear modulus, G is taken as 1/15 the modulus of elasticity, E (NZS3603, 1993) and the coefficient φ is given in Figure (2).

$$C = G\frac{hb^3}{\varphi}$$

Figure 2: Coefficient φ for computing torsional rigidity (Forest Products Laboratory 2010)

2.4.2 Timber Bearing Stiffness

The stiffness of a steel plate bearing on timber within a steel-timber connection is computed using a modulus of subgrade reaction, c, obtained from soil mechanics concepts according to Wanninger et al. (2015) as shown in Equation (11) where E_{90} is the elastic modulus perpendicular to the grain, b is the breadth of the timber being loaded. The subgrade reaction may be applied as an even distribution of springs spread over the loaded area to compute stresses and deformations. Wanninger et al. (2015) also propose that the end spring stiffness be increased to account for a 45-degree stress distribution. This better agrees with experimental results of timber bearing stiffness.

$$c = \frac{E_{90}}{b} \tag{11}$$

2.4.3 Casing Ends Stiffness

The flexural stiffness at the casing ends may be obtained experimentally. In the absence of experimental data, it may also be expressed assuming a reduced casing length. MacRae et al. (2022) proposes that for a lower bound stiffness, the casing length be reduced by the casing diameter/depth at either end of the casing.

3 METHODOLOGY

3.1 Glulam BRB Frame

For this study, the BRB in a timber frame by Dong (2021) was analysed. Three configurations, with different connection/gusset plate stiffeners, are analysed.

3.1.1 BRB Component Properties

The BRB system was split into seven components as shown in Figure 3. The components are the casing, top and bottom connection plates (TCP and BCP), top and bottom gusset plates (TGP and BGP), the portion of the gusset plates inserted into the timber beam (EGPB) and the portion of the gusset plate embedded into the foundation (EGPF). The unstiffened BRB component properties given in Table 1 include the second moment of area, I, the area, A, the section elastic modulus, Z, and the component length, L. For the casing, I and Z taken as that for the outer shell only as this dominates the behaviour (MacRae et al. 2022) and A, was determined using a transformed area approach. Section properties for the connection plates were determined by standard methods. Gusset plate properties were determined from the method shown in Section 2.3. Section properties of the gusset plate embedded into the timber section were approximated as the gusset plate properties plus the OOP timber beam properties. For the gusset plate embedded into the foundation, a large stiffness was assumed (MacRae et al. 2022). The BRB total length was 5.6m and the BRB maximum compression resistance, C_{max}, was 434kN.

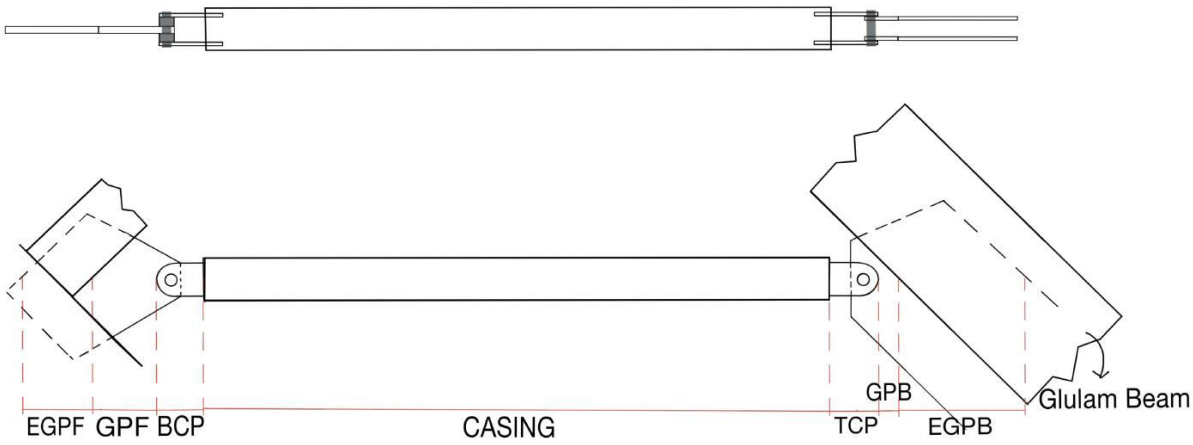

Figure 3: BRB example

Table 1. Unstiffened BRB component properties

Component	***Description***	***I (m^4)***	***A (m^2)***	***L(m)***	***Sum L (m)***	***Z (m^3)***
EGPF	Embedded gusset plate foundation	1.52E-02	1.97	0.32	0.32	9.72E-02
GPF	Gusset plate foundation	1.42E-06	0.013	0.36	0.68	8.80E-05
BCP	Bottom connection plate	2.93E-07	0.009	0.28	0.955	2.93E-05
CASING	Casing	3.01E-05	0.011	3.71	4.663	2.41E-04
TCP	Top connection plate	2.93E-07	0.009	0.28	4.938	2.93E-05
GPB	Gusset plate beam	2.85E-07	0.012	0.13	5.063	4.40E-05

EGPB	Embedded gusset plate beam	1.52E-03	0.2	0.55	5.613	9.72E-03

The moderately stiffened BRB had 40mm x 40mm (depth x breadth) rectangular stiffeners on each outer edge of the connection and top gusset plates. The bottom gusset plate used 20mm x 40mm stiffeners. The highly stiffened BRB used 80mm x 40mm stiffeners.

3.2 Rotational and Lateral Restraints

Due to the many uncertainties associated with modelling timber structures, a sensitivity analysis was conducted to capture the likely bounds of behaviour (Chen et al. 2022). The parameter varied was the rotational restraint where the BRB top connects to the timber beam. The rotational stiffness here is dependent on the timber connections, the timber beam torsional stiffness, and the slab. The top connection rotational stiffness, $K_{\theta,top}$ was calculated using Equation (12), where $K_{\theta,beam}$ is the beam torsional stiffness, $K_{\theta,beam\text{-}col}$ is the beam-column connection rotational stiffness, $K_{brace\text{-}beam}$ is the brace-to-beam gusset connection rotational stiffness, and $K_{\theta,slab}$ is the slab-to-beam connection rotational stiffness, if a slab is present. $K_{\theta,beam}$, $K_{\theta,beam\text{-}col}$ and $K_{\theta,brace\text{-}beam}$ acts in series while $K_{\theta,slab}$ acts in parallel. Locations of these rotational parameters are shown in Figure 4.

$$K_{\theta,TOP} = \frac{1}{\left(\frac{1}{K_{\theta,beam}} + \frac{1}{2K_{\theta,beam-col}} + \frac{1}{K_{\theta,brace-beam}}\right)} + K_{\theta,Slab} \tag{12}$$

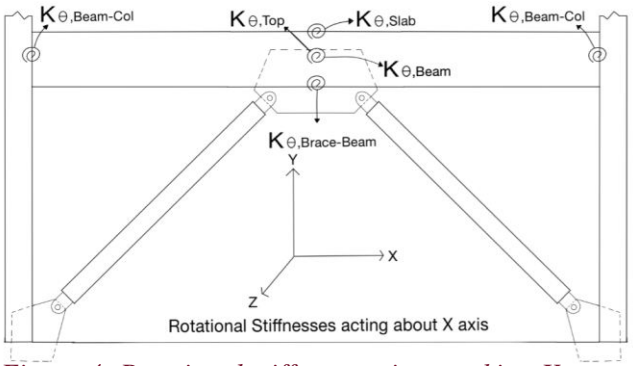

Figure 4: Rotational stiffness springs making $K_{\theta,top}$

The beam torsional stiffness, $K_{\theta,beam}$ was determined using the method proposed from the Wood Handbook (FPL, 2010) as discussed in Section 2.4.1. The connection rotational stiffnesses, $K_{\theta,beam\text{-}col}$ and $K_{\theta,brace\text{-}beam}$ were determined using FEM modelling, and they were compared with those from the elastic beam on foundation method which uses the timber bearing stiffness mentioned in Section 2.4.2. The BRB's modelled were assumed to have no slab restraint for simplicity.

A lower bound lateral restraint, computed as the timber beam OOP stiffness to an applied point load at mid-span according to Equation (13), using a 5th percentile modulus of elasticity for GL10 of E_{lb} = 7500MPa (NZS3603 1993), was considered for most analyses. The upper bound lateral restraint was assumed rigid.

$$K_{Lat} = \frac{48E_{lb}I}{L^3} = 1070kN/m \tag{13}$$

3.3 Connection Modelling

The timber beam-to-column connection rotational stiffness was modelled using both a beam-on-elastic-foundation (BOEF) method and Finite Element Modelling (FEM) software. The brace-to-beam connection was modelled with FEM due to its complex geometry being hard to replicate with the BOEF model. Both models involved applying a unit moment to the inserted plates, and measuring the rotation to obtain the rotational stiffness, k_θ, according to Equation (14) which is used to obtain $K_{\theta,top}$ in Equation (12).

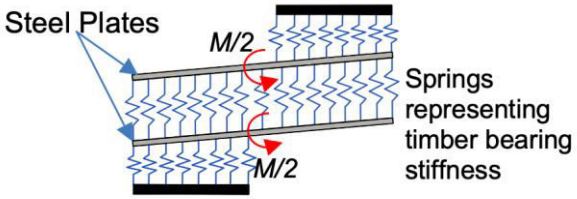

Figure 5: Beam on elastic foundation method

The BOEF method can be summarised as using springs to represent the Modulus of Elasticity of the timber perpendicular to grain, which is approximated as 1/30

the modulus of elasticity parallel to the grain as per Eurocode EN338 (2016). The rotational stiffness was calculated by applying a unit moment of rotation to the inserted plates as shown in Figure 5.

$$k_\theta = \frac{M}{\theta} \tag{14}$$

FEM software was used to obtain the beam-to-column connection, and brace-to-beam gusset connection, rotational stiffnesses, $K_{\theta,top}$. The timber sections were sized based on the frame tested by Dong (2021). For all timber sections, the material modulus of elasticity perpendicular to the grain, E_{90}, was used to model the elastic response. The steel plate was modelled as a non-deformable rigid element. The external faces of the timber sections were fixed to ensure that that the rotation obtained was only due to the plate embedding into the timber.

3.4 BRB Models and Analysis

The two analyses conducted were:

1) Axial buckling check

Elastic critical axial compressive force (i.e. buckling) analysis was conducted on a 2D single BRB using MASTAN2 to evaluate the brace buckling force, P_e, before completing the buckling check in Equation (2). The BRB casing was subdivided into 10 elements and an equivalent cantilever beam was applied at the end of the model to replicate the rotational spring stiffness of $K_{\theta,top}$ because MASTAN2 does not contain a rotational spring element. An equivalent axial member was applied at the top to replicate the lateral stiffness, K_{lat}.

Lower bound stiffnesses were used as they provide a conservative P_e estimate. To do this, the casing effective length was reduced by 1.0 times the depth of the casing (i.e. 250mm) at either end to model casing end flexibility as per Section 2.4.3. Lateral restraint, K_{lat} was 1070kN/m from Equation (13). The end rotational and lateral restraint of the brace-foundation connection will be 10 times the restraint of the brace to beam connection to replicate its high stiffness.

2) Combined axial/flexural check

Elastic analysis on a 3D Chevron BRB Frame to evaluate the combined axial/flexural check consider frame OOP deformations in Equation (4). The moment demands, M^*, could be evaluated using second order analysis to the expected OOP drifts. However, in this case they were conservatively estimated from the first order elastic analysis, to obtain M^*_1, and amplified to account for the axial force effect according to Equation (15).

$$M^* = \frac{M_1^*}{\left(1-\frac{C_{max,0}^*}{\phi P_e}\right)} \tag{15}$$

Upper bound stiffnesses were used as they cause larger moment demands. The bottom connection to the foundation was assumed fully fixed. The lateral restraint was assumed fully rigid. All connections between BRB components were assumed to be fully rigid (i.e the casing length is not reduced to replicate casing end flexibility). Displacement was applied at the frame first storey to various OOP drifts. Equivalent cantilevers were considered to provide the rotational stiffness, $K_{\theta,top}$.

4 BEHAVIOUR

4.1 Connection Modelling

Figures 7 shows the FEM analysis where a unit OOP moment, M_{OOP}, of 0.5kNm was applied to each plate.

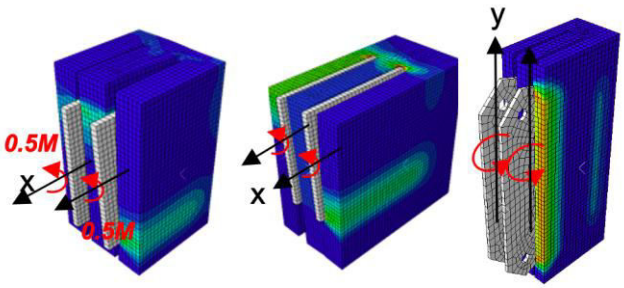

(a) Column (b) Beam (c) Brace to beam

Figure 7: Inserted plate timber connections subject to out-of-plane moment, M_{OOP}

Table 2 shows that the rotational stiffness, k_θ, values from the BOEF method are greater than those from the FEM analysis by between 12% and 38%. This is because the BOEF method treats the inner timber section between the two plates as being fixed at both ends. In reality (as shown in the Figure 7), the inner timber member has torsional flexibility and thus reduces the rotational stiffness of the connection. The beam-column connection stiffness, $K_{\theta,beam\text{-}col}$ is determined by combining $K_{\theta,beam,connection}$ (Figure 7b) and $K_{\theta,col,connection}$ (Figure 7a) as springs in series as:

$$K_{\theta,beam-col} = \frac{1}{\frac{1}{7140}+\frac{1}{9260}} = 4030kNm/rad$$

Table 2. Rotational stiffness of timber connections from figure 7, k_θ using FEM and beam on elastic foundation method

Method	$K_{\theta,col,connection}$ (a) (kNm/rad)	$K_{\theta,beam,connection}$ (b) (kNm/rad)	$K_{\theta,brace\text{-}beam}$ (c) (kNm/rad)
FEM	7,140	9,260	33,333
BOEF	8,820	12,800	-

4.2 BRB Analysis

4.2.1 Rotational Stiffness Bounds

Using Equation (10), the torsional rigidity, C, is 2700kNm^2 using the mean shear modulus, G, of 670MPa for the GL10 beam. Using the lower bound shear modulus of 500MPa for GL10 (E_{lb}/15 =7500MPa/15), C = 2030kNm^2. Beam torsional stiffness, $K_{\theta,beam}$ is determined using Equation (16) where the factor of 2 is to account for the beams on both sides of the brace intersection point, where L is half the beam length measured from the brace intersection point to the column face, of 3.84m. Therefore upper and lower bound rotational stiffnesses are $K_{\theta,beam,upper}$ = 1420 kNm/rad and $K_{\theta,beam,lower}$ = 1060kNm/rad respectively.

$$K_{\theta,beam} = \frac{2C}{L} \quad (16)$$

For the rotational stiffness at the top of the BRB, BRB frame upper bound analysis, the timber beam-column connections and brace to beam connection are assumed fixed. Lower bound analysis uses the rotational stiffness values, K_θ, from FEM with a stiffness reduction factor ϕ assumed as 0.5. This factor is for shrinkage effects and construction tolerances for timber connections. It also accounts for the likely pinched hysteretic behaviour of the timber connections resulting in larger connection rotations due to unrecoverable crushing of wood following multiple loading cycles (Chen et al. 2022). The upper and lower bound rotational stiffnesses are given in Equation (12).

$$K_{\theta,TOP,Lower} = \frac{1}{\left(\frac{1}{1060}+\frac{1}{2\phi\times4030}+\frac{1}{\phi\times33333}\right)} = 800kNm/rad$$

$$K_{\theta,TOP,Upper} = \frac{1}{(\frac{1}{1420}+\frac{1}{\infty}+\frac{1}{\infty})} = 1420kNm/rad$$

4.2.2 Parameter Checks

An initial parameter check was performed to check that $K_{\theta,top}$ is being applied accurately to the 3D frame model. An 8m beam was subject to torsion at mid-length (the location of the brace to beam connection). Cantilevers at each end of the beam represent the beam-column connection rotational stiffness. The moment applied, M, was equal to $K_{\theta,top}$. The resulting rotation at midspan was 1 rad, which indicates $K_{\theta,top}$ is being applied correctly to the 3D model considering Equation (14).

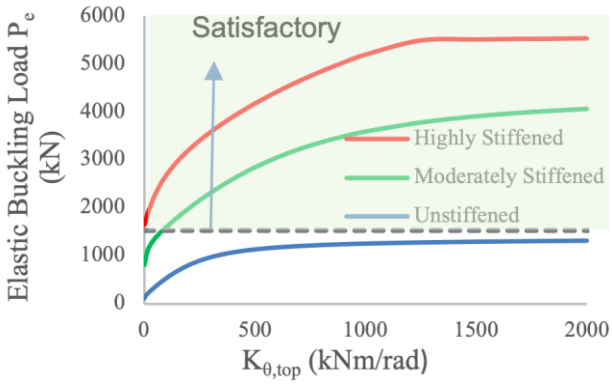

moderately stiffened BRB satisfies this requirement if $K_{\theta,top}$ greater than 80kNm/rad, and the highly stiffened BRB meets this criterion for all $K_{\theta,top}$.

4.2.3 BRB System Elastic Buckling Loads

The BRB system elastic buckling loads with varying top rotational stiffness were performed on the 2D model for the 3 BRB models. Figure 8 shows the elastic buckling load increases with increasing $K_{\theta,top}$. This indicates that it increases with gusset and connection plate stiffness. To satisfy the axial check in Equation (2), P_e must be greater than $C_{max}/0.285$ = 1520 kN as shown by the dashed line in Figure 8. The unstiffened BRB does not meet this criterion for any $K_{\theta,top}$ due to its high flexibility. The

Figure 8: Elastic buckling load vs top connection rotational stiffness for 3 BRB models

4.2.4 Combined Axial/Flexural Checks

The vertical dashed lines in Figure 9 show upper and lower bounds of $K_{\theta,top}$ (800 and 1420 kNm/rad) for the timber frame. They also show a horizontal dashed line when the Equation (4) ratio, $C_{max,0}/(\phi P_n) + M^*/(\phi M_n)$, is 1.0. The BRB passes combined actions checks only if all BRB component curves between the vertical dashed lines are below the horizontal dashed line. For all three BRB models, an OOP drift ratio of 1.5% (54mm) was applied at the beam top connection. For all three BRB's, a high ratio from Eq. 4 occurs at low $K_{\theta,top}$ stiffnesses because P_e decreases so $C_{max,0}/(\phi P_n)$ increases, and even though there are lower first order moments, the moment amplification from Equation (15) is large. This is more significant in the unstiffened BRB where P_e is smaller. For higher $K_{\theta,top}$ which satisfy axial checks $P_e > 0.285C_{max}$, the moment amplification is not as severe.

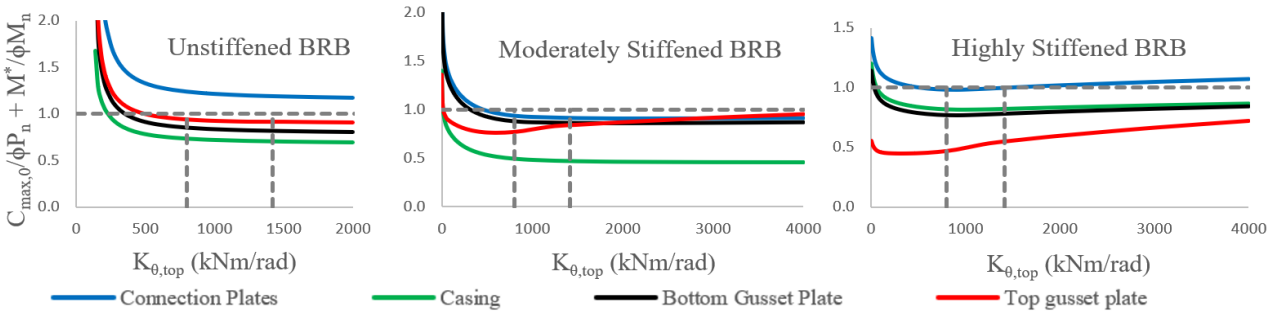

Figure 9: Combined criteria curves vs $K_{\theta,top}$ for the three BRB Models at 1.5% OOP drift

As expected, as $K_{\theta,top}$ increases, the moment demands in the BRB components increase, causing $M^*/\phi M_n$ to increase and the axial capacity of the components also increases causing larger P_e, a larger slenderness λ_n

from Equation (5), and a larger P_n causing $C_{max,0}/\phi P_n$ to decrease. This decrease in the first term of Equation (4) due to axial force, and the increase in the second term, due to moment, cause the total value from the Equation (4) interaction formula to not significantly change after $K_{\theta,top}$ of about 500 kNm/rad at this drift value.

Figure 9a shows that the BRB with *unstiffened plates* was too flexible, with relatively high demand-to-capacity ratios. At all ranges of $K_{\theta,top}$, including higher values than shown in the figure, the connection plate element never satisfies Eq. 4 under the bidirectional loading.

The BRB with *highly stiffened plates*, as shown in Figure 9c, satisfied Equation (4) over the range 800kNm < $K_{\theta,top}$ < 1,380 kNm.

The BRB with the moderately stiffened gusset plate proved to be the "sweet spot" in terms of gusset and connection plate stiffness. All BRB components satisfied Equation (4) when $K_{\theta,top}$ > about 500 kNm/rad as shown in Figure 9b. The critical element was the connection plate, with $C_{max,0}/(\phi P_n) + M^*/(\phi M_n) = 0.93 < 1$ at the lower bound $K_{\theta,top}$ of 800kNm/rad.

If slab restraint existed, fully restraining the beam in torsion (i.e. $K_{slab} = \infty$), fixed-fixed conditions should likely be assumed as an upper bound stiffness. If fixed-fixed conditions ($K_{\theta,top} = \infty$) and an upper bound stiffness are considered, then the BRB does not satisfy Equation (4) as $C_{max,0}/(\phi P_n) + M^*/(\phi M_n) = 1.16 > 1$. Gusset plate stiffener sizes and/or other BRB component stiffnesses should be reduced to allow for the larger lower and upper bounds of $K_{\theta,top}$ causing higher moment demands. This will achieve the new sweet spot of stiffness. The BRB models with highly stiffened and unstiffened gusset plates did not satisfy Equation (4) for fixed-fixed restraints either, with $C_{max,0}/(\phi P_n) + M^*/(\phi M_n)$ being 1.22 and 1.16 respectively.

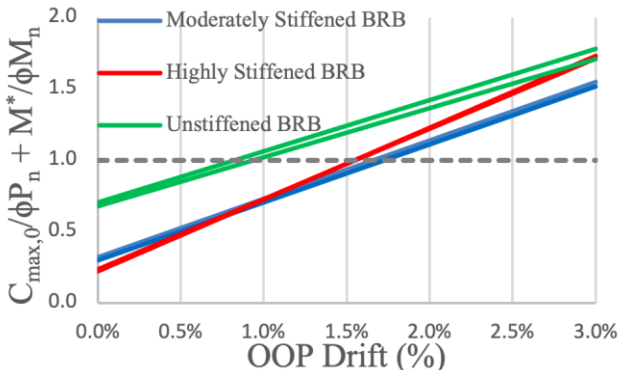

Figure 10: Combined action criteria vs OOP drift for the connection plates considering stiffness bounds

Figure 10 shows how each BRB performs for combined actions, according to Equation (4) at varying OOP drift. The connection plates were the critical element for all three BRB systems. The double lines show the lower and upper bounds of $K_{\theta,top}$. The BRB system with the moderately stiffened gusset plates indicated that yield would occur after a drift of 1.66%, while that with unstiffened gusset plates was 0.825%.

5 CONCLUSIONS

Models of BRB systems with timber frames in a chevron configuration were developed in order to assess their likely performance during strong bidirectional earthquake shaking. It was found that:

1) If a well-designed BRB satisfies (i) an axial stability check, and also (ii) a moment-interaction check, then buckling of the BRB system and yielding outside the core yield zone should not occur. While analysis tools are available to perform these analyses, the response depends on the properties of all the components of the BRB system. Some of these properties are not clear, including the rotational/lateral stiffness timber members, the stiffness of the timber-steel connections, the stiffness of the gusset plate and connection region at the end of the BRB, and the rotational restraint at the end of the BRB casing/restrainer. Methods are needed to evaluate these properties, or obtain reasonable bounds on them.

2) The rotational stiffness of the timber connections between the brace end and beam, as well as at the beam-column joint were obtained using finite element analysis (FEM). Also some beam-on-elastic-foundation (BOEF) modelling was performed. The BOEF and FEM results were consistent considering the differences in modelling assumptions made. Due the uncertainty associated with the material properties and modelling, upper and lower bound estimates of properties were considered.

3) When evaluating the BRB system axial stability, and likelihood of yield outside the core within the casing, the connection and gusset plate stiffness are important. It was shown that the best performance for a certain out-of-plane drift ratio may be obtained when the connection/gusset plate stiffness is not too high or too low.

4) Based on the findings above, for timber frames with chevron BRBs subject to bidirectional shaking causing both in-plane and out-of-plane frame deformations, both the BRB system axial stability, and the likelihood of BRB system yield outside the core yield zone may be simply evaluated.

6 REFERENCES

AISC341-16. (2016), Seismic Provisions for Structural Steel Buildings. AISC. Chicago, USA.

CEN, EN 338. (2016), Structural Timber - Strength classes. European Committee for Standardization.

Chen. Z, Tung. D, Karacabeyli, E. (2022) *Modelling Guide for Timber Structures,* FPInnovations.

Cui, J. (2021). "BRB Performance Issues." University of Canterbury.

Dong, W. (2021). "Seismic Performance of glulam frames with buckling restrained braces (BRBs)." University of Canterbury.

Forest Products Laboratory. (2010). *Wood Handbook: wood as an engineering material,* Forest Products Society.

MacRae. G. A, Lee. C-L. (2022). "BRB System Design Considerations." *NZSEE.* Draft to be submitted in 2022, obtained by personal communication with the first author.

NZS 3404. (1997), Part 1: 1997 – Steel Structures Standard. Standards New Zealand. Wellington, New Zealand.

NZS 3603. (1993), Timber Structures Standard. Standards New Zealand. Wellington, New Zealand.

Wanninger. F, Frangi. A, Steiger. R. (2015). "Bearing stiffness in wood-to-wood compression joints." *Engineering structures,* 631-640.